Vietnam Journal of Catalysis and Adsorption
Tạp chí xúc tác và hấp phụ Việt Nam

https://chemeng.hust.edu.vn/jca/

Development of quantitative ion physic chemistry properties-activity relationship (QIPAR) and docking simulation for sars-covid-2 protein

Pham Van Tat[1*], Nguyen Minh Quang[2], Bui Thi Phuong Thuy[3], Tran Thai Hoa[4], Nguyen Thanh Duoc[5]

[1]*Institute of Development and Applied Economics, Hoa Sen University, VIETNAM*
[2]*Faculty of Chemical Engineering, Industrial University of Ho Chi Minh City, VIETNAM*
[3]*Faculty of Basic Sciences, Van Lang University, VIETNAM*
[4]*Department of Chemistry, University of Sciences, Hue University, Hue, VIETNAM*
[5]*Faculty of Pharmacy, Hong Bang International University, VIETNAM*
**Email: vantat@gmail.com*

ARTICLE INFO

Received: 10/5/2021
Accepted: 10/8/2021
Published: 15/10/2021

Keywords:

SARS-CoV-2; hybrid QIPAR models; docking simulation; Ion-Binding Site

ABSTRACT

Currently, many drugs are being studied and potentially used in the treatment of SARS-CoV-2. Compounds studied are mostly organic substances. This work investigates the ability to inhibit SARS-CoV-2 of various 20 metal ions based on their ability to inhibit several biological systems; the physicochemical properties of metal ions were calculated by quantum chemistry DFT (B3LYP/ LanL2DZ) were used to develop the QIPAR hybrid models. Hybrid models QIPARGA-MLR (k = 4) and QIPARGA-ANN with architecture I(4)-HL(9)-O(1) were developed to predict the biological activity of metal ions. Metal ions were also investigated for their inhibitory potential for the protein SARS-CoV-2 (PDB6LU7) by docking simulation techniques. We predicted the binding sites of metal ions to the active sites of the SARS-CoV-2 protein (PDB6LU7). These studies are consistent with their activities against different biological systems. This research will also contribute to the development of metal oxide nanomaterials.

Introduction

SARS-COVID-19, caused by coronavirus-2 (SARS-CoV-2) that spread to many countries, created a pandemic worldwide. It affects hundreds of millions of lives. China has shared clinical practice and provided investigations in the fierce battle against the COVID-19 virus. Dan Zhang et al. provided detailed information on clinical applications against the COVID-19 virus [1]. Several drugs are proven to be clinically effective against SARS-CoV-2, such as the drugs Azithromycin and Nitazoxanide [2]. From the structural and functional relationships that can synthesize these drugs, Mina T. Kelleni recommends using these two drugs in combination as soon as possible in the clinical course of COVID-19 [2]. However, the vaccine against the virus is still in the testing process, and there are several drugs in the experimental stages that inhibit the infection and replication of SARS-CoV-2 [3]. Furthermore, the other chloroquine, hydroxychloroquine, and other antiviral drugs identified by Dwight L. McKee et al., such as the nucleotide analog remdesivir, maybe HIV protease inhibitors lopinavir and ritonavir. To date, broad-

https://doi.org/10.51316/jca.2021.087

spectrum antiviral drugs, such as arbidol, favipiravir, and antiviral phytochemicals, have shown the ability to limit infection SARS-CoV-2 [3]. Chemical composition and pharmacological mechanism analysis of Qingfei Paidu Decoction (QFPD) studied by Ruocong Yang et al. used to treat COVID-19 patients in China [4]. Qianwen Zhao et al. studied and explored the relationship between the lymphocyte count and the severity of SARS-COVID-19 [5]. The COVID-19 drug discovery and testing efforts incorporate experimental methods and computer simulation techniques of the transmission mechanism of the human SARS-CoV-2 virus proposed by Jian Shang et al [6]. During the current pandemic, efforts to locate broad-spectrum antiviral agents pose a significant challenge. Using in silico modeling techniques and supporting data analysis and prediction of protease inhibitors SARS-CoV-2, Kalyan Ghosh et al. have developed several models based on Monte Carlo optimization techniques for screening natural products [7]. Ulf Norinder et al. have identified 36 compounds that may have antiviral effects against coronavirus using an in *silico* model that predicts lysosome accumulation [8]. Based on the photoelectric and spectral properties of molecules resistant to SARS-CoV-2, G.W. Ejuh et al. summarized and evaluated the critical role of molecular descriptors for building models (QSAR) and designing molecules electronegativity index, global hardness potential, ionization potential, electronic affinity [9].

There are also many efforts to introduce COVID-19 treatments in Vietnam, but there are no drugs to treat coronavirus respiratory infections. This still has potential complications and risks. Also, in Vietnam, many studies combine empirical and *silico* modeling done by Thuy et al. with the SARS-COV-2 virus by docking simulation using ingredients of essential garlic oil [10]. In another study on natural tea tree oil in Vietnam, Ai Nhung et al. carried out a docking simulation to determine the inhibitory ability of the virus SARS-CoV-2 [11]. To perform docking simulations and to look for different types of compounds to prevent SARS-CoV-2 infection, Ai Nhung et al. investigated the use of silver and bis-silver complexes with lighter tetrylene. They demonstrated the potential of using silver-carbene and bis-silver-carbene complexes to inhibit the SARS-CoV-2 virus infection [12].

There are many reasons to explain the earlier effects in the treatment of SARS-COV-2 patients in Viet Nam. Many drugs and regimens used by Vietnamese doctors to treat patients with respiratory tract infections are similar to those used to treat HIV patients. Another treatment has shown that the use of chloroquine and an antibiotic can also treat the SARS-CoV-2 virus. However, all these drugs are still in the research and development phase. In addition, the discovery of a new drug and inhibitory mechanism for the SARS-COV-2 still requires much research.

From studies on SARS-CoV-2, we realize a need to continue building the in silico models based on molecular descriptors. We now find that the individual metal ions can also inhibit the proteins of various infectious viruses [13]. This will also be an essential research direction and play an essential role in developing new nano oxide material drugs for the treatment [14,15]. Furthermore, inorganic nanomaterial compounds of metal ions with diverse biological activity are also studied [15]. The *in silico* models based on simulation techniques are still the main focus today, providing more reliable predictability [16,17].

This work was to select a group of biologically active metal ions Hg^{+}, Ca^{2+}, Cd^{2+}, Cu^{2+}, Mg^{2+}, Mn^{2+}, Ni^{2+}, Pb^{2+}, Zn^{2+}, Co^{2+}, Cr^{3+}, Fe^{3+}, Cs^{+}, K^{+}, Sr^{2+}, Li^{+}, Na^{+}, Ba^{2+}, La^{3+}, Ag^{+} [14,15] to probe for potential inhibition of SARS-CoV-2 infection. We used the metal ion descriptor received by the method DFT (B3LYP/LanL2DZ) to develop a hybrid QIPAR model based on multivariate linear regression ($QIPAR_{GA-MLR}$) and artificial neural network ($QIPAR_{GA-ANN}$). The correlation between metal ion structure and SARS-CoV-2 inhibitory activity was determined based on the most reliable QIPAR models. Metal ions were discovered for SARS-CoV-2 inhibitory activity by simulating docking to attach metal ions to the SARS-CoV-2 receptors (PDB6LU7) [18]. Predict possible sites to bind metal ions on receptors of the SARS-CoV-2 protein. We evaluated the electrostatic interaction and complexing properties of metal ions with amino acids at active sites on the SARS-CoV-2 protein. Active metal ions can be important contributors to the fabrication of new bioactive nanomaterials.

Experimental

Data set

In recent studies, 20 metal ions have been shown to have inhibitory abilities against Bacterial bioluminescence [14]. Besides, it is shown that metal ions can also inhibit any nucleic acid other than polymerase. Therefore, a structural activity relationship (QIPAR) study of SARS-CoV-2 inhibitory metal ions is

needed. Group of metal ions and bacteria inhibitory concentration 50% (EC_{50}, μM) are obtained from various works [14-22]. The EC_{50} value indicates inhibitor concentration in μM. The inhibitory activity pEC_{50} = -logEC_{50} is shown in Table 1. The data group was divided into 70% training group, 15% validation group, and 15% testing group, as shown in Table 1.

Table 1: The metal ions correspond to experimental inhibitory activity $pEC_{50,exp}$[14-22], and those from the hybrid QIPAR models

STT	Metal ions	$pEC_{50,exp}$	$QIPAR_{GA-MLR}$		$QIPAR_{GA-ANN}$	
			$pIC_{50,cal}$	Residuals	$pIC_{50,cal}$	Residuals
1^{tr}	Hg^{+}	1.160	0.998	0.162	1.004	0.156
2^{te}	Ca^{2+}	-0.990	-0.822	-0.168	-0.888	-0.102
3^{tr}	Cd^{2+}	0.170	0.256	-0.086	0.324	-0.154
4^{tr}	Cu^{2+}	0.650	0.571	0.079	0.719	-0.069
5^{va}	Mg^{2+}	-1.020	-0.561	-0.459	-0.957	-0.063
6^{tr}	Mn^{2+}	-0.200	-0.520	0.320	-0.215	0.015
7^{tr}	Ni^{2+}	0.290	0.148	0.142	0.312	-0.022
8^{te}	Pb^{2+}	0.460	0.752	-0.292	1.142	-0.682
9^{tr}	Zn^{2+}	-0.090	0.174	-0.264	-0.108	0.018
10^{va}	Co^{2+}	0.270	0.152	0.118	0.139	0.131
11^{tr}	Cr^{3+}	0.020	-0.005	0.025	-0.019	0.039
12^{tr}	Fe^{3+}	0.340	0.246	0.094	0.309	0.031
13^{tr}	Cs^{+}	-0.630	-0.779	0.149	-0.645	0.015
14^{tr}	K^{+}	0.730	0.732	-0.002	0.743	-0.013
15^{va}	Sr^{2+}	-0.880	-0.854	-0.026	-0.851	-0.029
16^{tr}	Li^{+}	-0.970	-1.035	0.065	-0.958	-0.012
17^{tr}	Na^{+}	-0.800	-0.958	0.158	-0.919	0.119
18^{tr}	Ba^{2+}	-0.760	-0.765	0.005	-0.811	0.051
19^{te}	La^{3+}	-0.530	-0.427	-0.103	-0.737	0.207
20^{tr}	Ag^{+}	0.840	0.757	0.083	0.924	-0.084
RMSD value				0.180		0.176

tr: training set; va: validation set; te: test set

Calculating the molecular descriptor

The hybrid QIPAR model with a predictive quality of efficiency, characteristic metal ion descriptors were calculated from DFT B3LYP/LanL2DZ in the Gaussian09 program [21]. They are essential for the development of QIPAR in silico models. To develop QIPAR models, different descriptors Atomic Weight (AW), Atomic Radius (AR), Heat of Fusion (HF), Electronegativity (EN), first ionization potential (IP1), second ionization potential (IP2), pH, covalence index (COVAL), ionic index (ION), the softness index (SOFT), an atomic number divided by the difference in ionization potentials for the ion oxidation numbers (ANIP), the log of ANIP (LGANIP), the difference in electrochemical potential (DELE), hydrolysis constant (HYD) and total dissolved metal (TOTLEC) [14,15]. These descriptors have a significant influence on the properties of metal ions. They have specifically altered the binding to the protein activity sites PDB(6LU7) of the SARS-CoV-2 virus.

Building QIPAR model

$QIPAR_{GA-MLR}$ model

In the general case, the coefficients in the multivariable linear regression model $QIPAR_{GA-MLR}$ characterize the contribution to pEC_{50} activity [14,15]. The general model $QIPAR_{GA-MLR}$ is shown as follows [23,25]:

$$y = b_0 + \sum_{i=1}^{k} b_i x_i \quad (1)$$

The observed values y_i for a compound are approximately represented by the linear combination of molecular descriptors x_i. The characteristic coefficients for that association are called the

regression coefficients b_i [25]. The significance of these coefficients in the QIPAR$_{GA-MLR}$ model is evaluated based on multiple correlation coefficient (R^2), cross-validation Q^2_{LOO} (leave-one-out) (Eqs. (2)), adjusted correlation coefficient R^2_{adj} (Eq. (8)), and significance level (p-value) [25,26]. The statistical parameters are calculated by the following equations [23,25]:

$$R^2 = 1 - \frac{\sum_{i=1}^{n}(y_i - \hat{y}_i)^2}{\sum_{i=1}^{n}(y_i - \bar{y})^2} \quad (2)$$

Where y_i and $\hat{y}_i$ are the experimental and prediction values

$$R^2_{adj} = 1 - \left[\frac{(n-1)\times(1-R^2)}{N-k-1}\right] \quad (3)$$

The RMSD error values validate the predictive quality of pEC_{50} of the QIPAR models for the training group, validation group, and test group [26]. The prediction error of the RMSD is calculated by the equation (4):

$$RMSD = \sqrt{\frac{\sum_{i=1}^{n}\left(\hat{y}_i - y_i\right)^2}{n}} \quad (4)$$

As we all know, the selection of metal-ions descriptors for the QIPAR$_{GA-MLR}$ model is becoming very important in analysis, molecular design, and activity prediction pEC_{50}. The Genetic Algorithm (GA) is one of the most widely used and most effective current priority algorithms for selecting the metal-ions descriptors. Furthermore, the hybrid QIPAR model of multivariate regression is built from selected variables by a genetic algorithm [24] called the QIPAR$_{GA-MLR}$ model.

The quality of training and predictability of the QIPAR$_{GA-MLR}$ model in Table 1 were compared based on the Residuals values. The value Q^2_{LOO} (the statistical value assessed by the method leave-one-out). We found that the QIPAR$_{GA-MLR}$ model with k = 4 seemed to be the most suitable, and the QIPAR$_{GA-MLR}$ model can be chosen for the following prediction.[23-26] This can also be seen in Fig 3b. This QIPAR$_{GA-MLR}$ model has good predictability as well:

$$pEC_{50} = -3.3557 + 0.5099\times AR - 0.1456\times TOTLEC + 1.0170\times EN + 0.2390\times pH \quad (5)$$

Where n = 14; R^2 = 0.928; R^2_{adj} = 0.909; Q^2_{LOO} = 0.759; F-value = 48.2848; p-value is in range 0.000 to 0.0240 at 95% confidence level for metal-ions descriptors included in QIPAR$_{GA-MLR}$ model.

The training set can be well described by the QIPAR$_{GA-MLR}$ regression equation (5). It did appear to be very statistically significant. The leave-one-out cross-validation (LOO) technique is also the basis for choosing the built-in QIPAR$_{GA-MLR}$ model to meet the actual requirement to predict the pEC_{50} value. The QIPAR$_{GA-MLR}$ model with k = 4 (in Table 1).

QIPAR$_{GA-ANN}$ model

A neural network architecture consists of some layers, each consisting of some neurons [17,27]. First, the artificial neural network structure is built following the natures of the metal ions. Then, we can apply artificial intelligence techniques to find the most suitable network architecture. At this stage, the neural network nodes apply an iterative process of the number of molecular descriptors (input variables) to adjust the weights for optimal prediction.

However, the relationships between the descriptors and activity pEC_{50} cannot be expressed clearly in the traditional models. We used the neural network architecture I(k)-HL(m)-O(1). Here I(k) is the input layer with k = 4 descriptors or the number of neurons on the input layer as defined in the QIPAR$_{GA-MLR}$ model (5); layer HL(m) is the hidden layer with m = 9 neurons; layer O(1) is the output layer with one neuron corresponding to pEC_{50} activity in the QIPAR$_{GA-MLR}$ model. The neural network is considered good training results when the difference between the target t_i and the prediction values y_i is the smallest. This is called the sum of squared residuals (SSR) [16]:

$$SSR = \sum_{i=1}^{n}(y_i - t_i)^2 \quad (6)$$

with $i = 1 - n$ (n is the number of training cases)
These techniques may require fewer iterations to train an artificial neural network based on fast convergence rates and smarter search criteria. n = 14; R^2 = 0.981; R^2_{adj} = 0.909; Q^2_{LOO} = 0.981; R^2_{pred} = 0.955; the results are showed in Table 1. The parameters are used as the training algorithm BFGS 6; Error function SOS; logistic activation function, and Identity activation function. The training error is 0.0088, and the test error is 0.0036; a validation error is 0.072 at a 95% confidence level for metal-ions descriptors included in the QIPAR$_{GA-MLR}$ model.

Docking simulation

The Protein Data Bank provided the experimental structure of the SARS-CoV-2 (6LU7) protein [18]. RCSB

PDB data is built on experimental data by generating resources for molecular biology research. Many different metal ions can bind to various active positions of different proteins. Metal ions bind to proteins by the most common bonds, such as coordination bonds with amino acids, electrostatic bonds, and van der Waals bonds. The most common metal ions, such as iron, are abundant in biological systems. Iron ions have an essential function in physiological processes. However, metal ions bind to active sites of many proteins that are not well understood about biological function. Therefore, it is crucial to determine the critical active sites on proteins to predict the biological activity of metal ions.

Table 2: Metal ions bound to amino acids of A SARS-CoV-2 protein chain PDB6LU7 examined and metal ion-binding residues

Metal ion	Simulation method binds metal ions		Metal ion	Predicting for binding positions	
	Binding Residues patterns	Residue Number		Binding Residues patterns	Residue Number
Cu^{2+}	17	30	Pb^{2+}	12	22
Ca^{2+}	13	26	Cr^{3+}	10	17
Fe^{3+}	12	23	Cs^{+}	7	13
Fe^{2+}	40	25	K^{+}	8	19
Mg^{2+}	13	19	Sr^{2+}	10	18
Mn^{2+}	7	14	Li^{+}	6	12
Zn^{2+}	11	16	Na^{+}	9	15
Cd^{2+}	5	10	Ba^{2+}	12	20
Ni^{2+}	6	13	La^{3+}	13	24
Hg^{2+}	10	22	Ag^{+}	6	13
Co^{2+}	14	22			

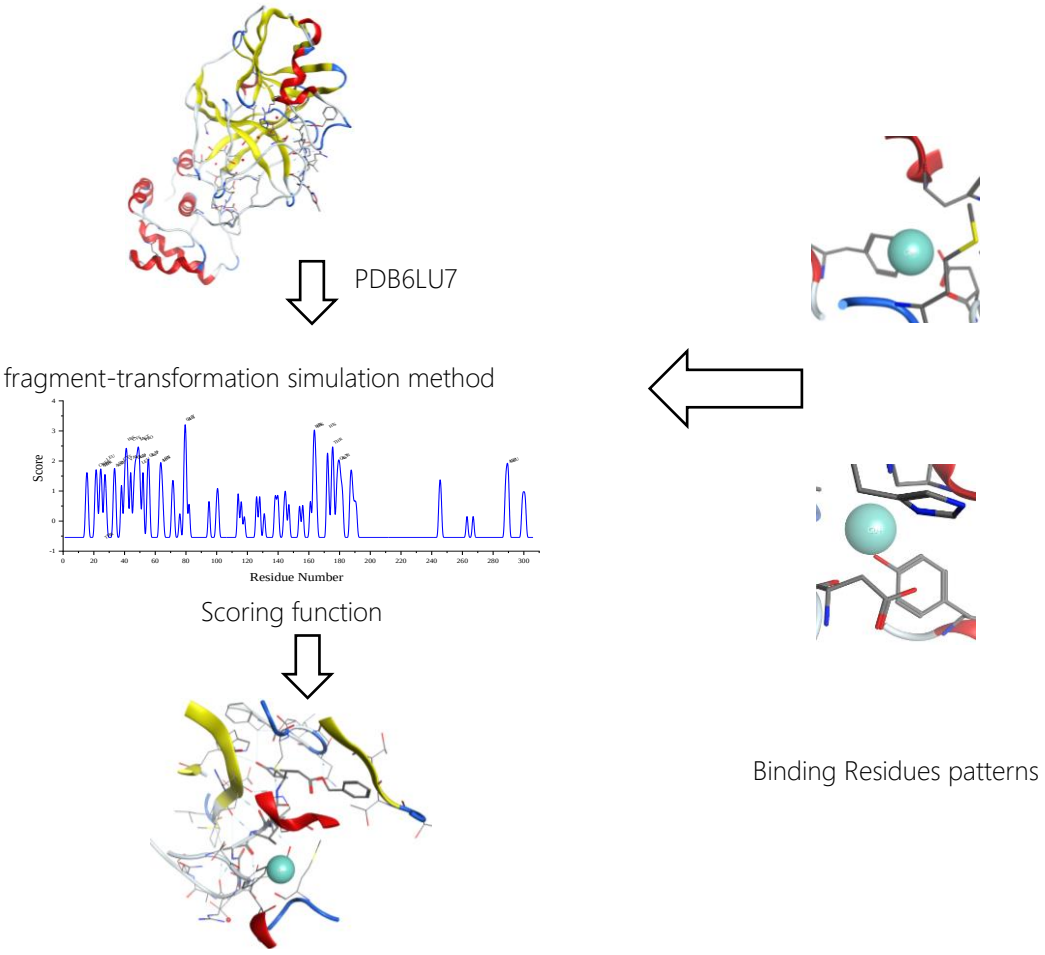

Figure 1: The metal ion–binding prediction method

https://doi.org/10.51316/jca.2021.087

The 3-dimensional space of the active site needs clarification of the ions' binding properties to proteins, which will provide more explicit information about the possible influence of metal ions concerning protein function. Usually, protein structures determine the functions of biological systems such as bacteria and viruses. Primarily when it interacts with metal ions and interacts with other components, the metal ions can stabilize the protein structure and catalyze in biological reactions or alter the biological properties of proteins, such as inhibiting the proliferation of viruses; Identifying metal ion binding sites with proteins is the key to understanding the biological relevance of metal ion binding proteins. Meanwhile, the experimental path is complicated to determine metal bonding sites because this process requires very complex steps or specialized techniques, such as nuclear magnetic resonance spectroscopy, electrophoresis, metal affinity column chromatography, and electrophoresis displacement assays, and absorption spectroscopy.

In contrast, simulation methods can allow the quick and easy identification of metal-to-protein binding sites. Furthermore, this method is usable with large databases and has an accessible protein structure in the Protein Data Bank (PDB) [18].

However, we use the PDB6LU7 protein of SARS-CoV-2 and to determine the binding sites of metal ions. The fragment-transformation simulation method binds metal ions such as Ca^{2+}, Cu^{2+}, Fe^{3+}, Mg^{2+}, Mn^{2+}, Zn^{2+}, Cd^{2+}, Fe^{2+}, Ni^{2+}, Hg^{2+}, and Co^{2+} PDB6LU7 protein of SARS-CoV-2, as given in Table 2. This method allows predicting not only 11 binding positions with those metal ions and predicting for binding positions with ten other metal ions such as Pb^{2+}, Cr^{3+}, Cs^{+}, K^{+}, Sr^{2+}, Li^{+}, Na^{+}, Ba^{2+}, La^{3+}, and Ag^{+}. This simple method does not need to use practice data to predict and does not require complex force fields to calculate. Furthermore, this pathway allows us to elucidate the metal-binding sites in the 6LU7 protein and enrich the activity studies for the SARS-CoV-2 (PDB6LU7) protein.

Binding Site Prediction

The fragmentation simulation method is used to predict the exact binding sites of metal ions to the receptor of the SARS-CoV-2 protein 6LU7. A binding site assigns each residue of the query protein 6LU7 SARS-CoV-2. When the residue-bond point is higher than the specified threshold, this residue can be predicted as metal bond residue. Based on the 3D structure between the 6LU7 protein, the metal ions in the metal bonding template can be converted into the query protein structure. The 6LU7 protein complex structure with at least one ion Ca^{2+}, Cu^{2+}, Fe^{3+}, Mg^{2+}, Mn^{2+}, Zn^{2+}, Cd^{2+}, Fe^{2+}, Ni^{2+}, Hg^{2+}, Co^{2+} is described in Figure 1.

Metal-bonding residue patterns are extracted from the proteins that bind these metal ions. The metal-binding site must contain one metal ion and two radicals to qualify as a metal ion residual sample. Table 1 presents the statistics for the polypeptide chain of 6LU7 SARS-CoV-2 metal ion-bound and each metal bonded pattern. The metal-bound polypeptide chain of 6LU7 is defined by a protein chain that interacts with a specific metal ion.
Ten metal ions Pb^{2+}, Cr^{3+}, Cs^{+}, K^{+}, Sr^{2+}, Li^{+}, Na^{+}, Ba^{2+}, La^{3+}, and Ag^{+} can be selected to predict the bonding position according to the principle of Fig 1. The docking results are shown in Fig. 2a. The bonding scores of all residues are listed in the order that residues appear in sequence. The predicted metal ionic bonding residues are represented by a rod diagram identifying the associated amino acid radicals displayed, as shown in Fig 2b. It also allows the prediction of the binding position of the Metal ions in the 6LU7 protein structure. Finally, all-metal ion binding scores with residues of the entire query 6LU7 protein are displayed. It provided the predicted distribution of the bonding scores.

https://doi.org/10.51316/jca.2021.087

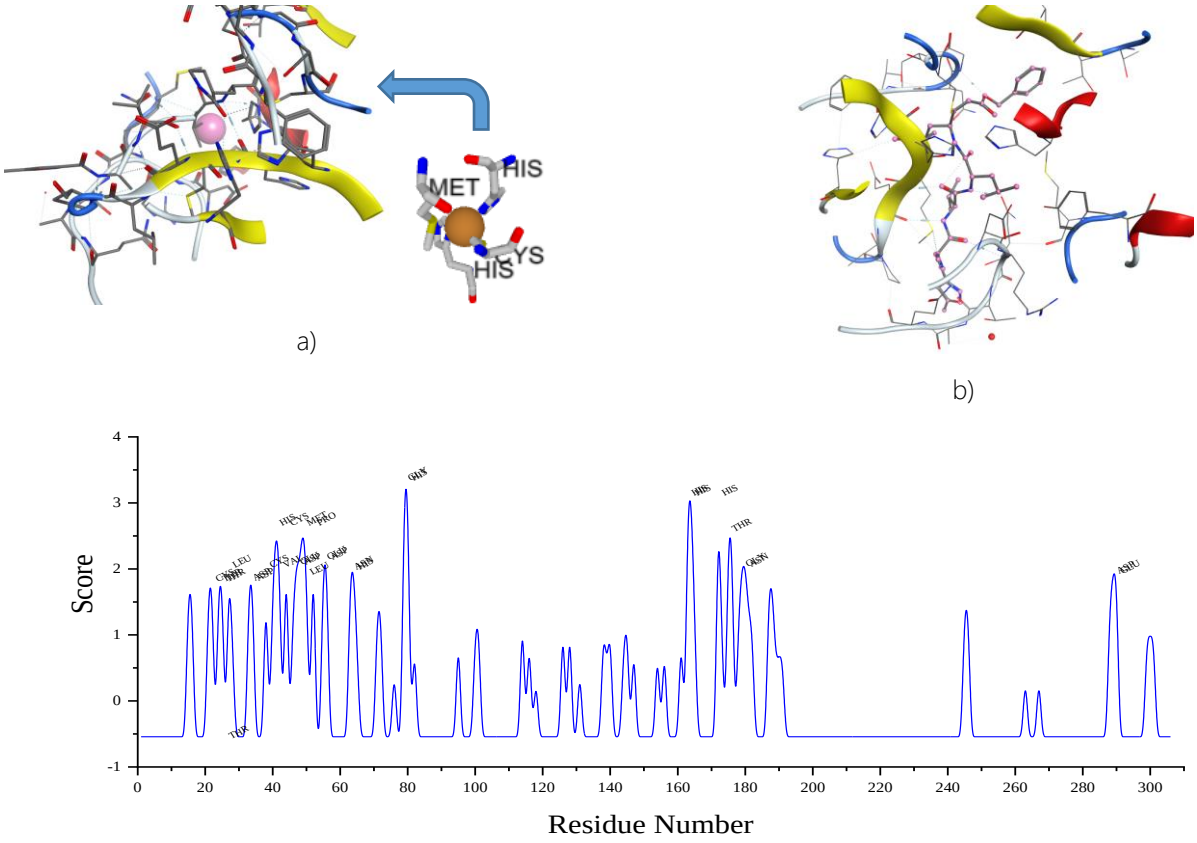

Figure 2: The predicted metal ion-binding residues for Pb^{2+} and shown as sticks in the 3D representation. a) docking site of Pb^{2+}; b) amino acid radicals sites; c) docking scores

Results and discussion

The ionic-active chemical and physical properties (QIPAR) relationships have been developed here based on the metal-to-protein binding natures. The $QIPAR_{GA-MLR}$ hybrid models were screened based on genetic algorithms and statistical parameters. $QIPAR_{GA-MLR}$ model gives predictive results consistent with the experimental results. Model $QIPAR_{GA-MLR}$ with the known number k = 4 is the basis for $QIPAR_{GA-ANN}$ model construction. Model $QIPAR_{GA-ANN}$ with architecture I(4)-HL(9)-O(1) gives better predictive results than the $QIPAR_{GA-MLR}$ model with error RMSD = 0.176. The training, rating, and test results from both QIPAR models are satisfactory for the EC50 prediction. The activity of metal ions against bacteria was accurately predicted from selected most essential properties such as atomic radius, the electronegativity of metals, total dissolution metal, and pH medium.

From the QIPAR model, we know the biological properties of a metal ion. Nevertheless, to get a more accurate view of the activity of metal ions. We performed a technique that simulates fragmentation and predicts metal ion binding sites to the receptor protein PDB6LU7 of SARS-CoV-2. We have also determined the active position on the protein 6LU7 that metal ions can bind to through simulation results. The receptors are 3D spatial locations with different sizes and amino acids that can coordinate with metal ions. Each metal ion can be directed to various positions on the 6LU7 protein chain. This depends on two critical properties of metal ions, such as the atomic radius and electronegativity. The docking simulation results and the QIPAR model gave consistent results about the activity nature of metal ions. In particular, we have thoroughly investigated the properties of metal ions for the inhibitory ability of SARS-CoV-2. These are the initial research results on the activity of metal ions on the 6LU7 protein of SARS-CoV-2.

Conclusion

Our research has successfully built a hybrid model, QIPARGA-MLR and QIPARGA-ANN. We also successfully docked the essential metal ions into the

https://doi.org/10.51316/jca.2021.087

receptor of the 6LU7 protein of SARS-CoV-2. We also predicted the binding sites of metal ions on the residue of the 6LU7 protein. This will help research the synthesis of nanomaterials with antiviral activity of SARS-CoV-2 from suitably blended metal oxides.

References

1. D. Zhang, B. Zhang, J. Lv, R. Sa, X. Zhang, Z. Lin, Pharmacological Research 157 (2020) 104882. https://doi.org/10.1016/j.phrs.2020.104882
2. M. T. Kelleni, Pharmacological Research 157 (2020) 104874. https://doi.org/10.1016/j.phrs.2020.104874
3. D. L. McKee, A. Sternberg, U. Stange, S. Laufer, C. Naujokat, Pharmacological Research 157 (2020) 104859. https://doi.org/10.1016/j.phrs.2020.104859
4. R. Yang, H. Liu, C. Bai, Y. Wang, X. Zhang, R. Guo, S. Wu, J. Wang, E. Leung, H. Chang, P. Li, T. Liu, Y. Wang, Pharmacological Research 157 (2020) 104820. https://doi.org/10.1016/j.phrs.2020.104820
5. Q. Zhao, M. Meng, R. Kumar, Y. Wu, J. Huang, Y. Deng, Z. Weng, L. Yang, International Journal of Infectious Diseases 96 (2020) 131–135. https://doi.org/10.1016/j.ijid.2020.04.086
6. J. Shang, G. Ye, K. Shi, Y. Wan, C. Luo, H. Aihara, Q. Geng, A. Auerbach, F. Li, Nature 581 (2020) 221–224.
7. K. Ghosh, A. Amin, S. Gayen, T. Jha, Journal of Molecular Structure 1224 (2021) 129026. https://doi.org/10.1016/j.molstruc.2020.129026
8. U. Norinder, A. Tuck, K. Norgren, V. M. Kos, Biomedicine & Pharmacotherapy 130 (2020) 110582. https://doi.org/10.1016/j.biopha.2020.110582
9. G. W. Ejuh, C. Fonkem, Y. T. Assatse, R. A. Y. Kamsi, T. Nya, L. P. Ndukum, J. M. B. Ndjaka, Heliyon 6 (2020) e04647. https://doi.org/10.1016/j.heliyon.2020.e04647
10. T. P. T. Bui, T. A. M. Tran, T. T. H. Nguyen, T. H. Le, T. H. Tran, T. P. L. Huynh, T. T. Nguyen, T. V. A. Tran, T. Q. Phan, V. T. Pham, V. H. Nguyen, T. Q. Duong, T.T. Nguyen, T. T. Vo, K. H. LaM, T. A. N. Nguyen, ACS Omega 5(14) (2020) 8312–8320. https://doi.org/10.1021/acsomega.0c00772
11. T. A. M. Tran, T. P. L. Huynh, T. T. H. Nguyen, T.H. Le, T. H. Tran, T. P. T. Bui, T. Q. Duong, T. T. Nguyen, T. V. A. Tran, T. X. D. Nguyen, T. T. Nguyen, V. H. Nguyen, V. T. Pham, T. T. Vo, T. A. N. Nguyen, Biological Chemistry & Chemical Biology 5(21) (2020) 6312-6320. https://doi.org/10.1002/slct.202000822
12. Q. B. Thanh, T. P. L. Huynh, T. A. M. Tran, T. Q. Duong, T. P. T. Bui, D. N. Vo, T. Q. Phan, V. T. Pham, Q. D. Duy, T. T. Nguyen, K. H. Lam, T. A. N. Nguyen, RSC Advances, 10 (2020) 30961-30974. https://doi.org/10.1039/D0RA05159D
13. C. Can, W. Jianlong, Chemosphere 69(10) (2007) 1610–1616. https://doi.org/10.1016/j.chemosphere.2007.05.043
14. J. T. Mccloskey, M. C. Newman, and S. B. Clark., Environmental Toxicology and Chemistry 15(10) (1996) 1730–1737. https://doi.org/10.51316/jca.2021.087
15. J. Ying, T. Zhang, M. Tang, Nanomaterials 5 (2015) 1620-1637. https://doi.org/10.3390/nano5041620
16. K. Roy, Advances in QSAR Modeling Applications in Pharmaceutical, Chemical, Food, Agricultural and Environmental, Springer International Publishing AG, Gewerbestrasse 11, 6330 Cham, Switzerland, 2017.
17. T. Engel, J. Gasteiger, Applied Chemoinformatics: Achievements and Future Opportunities, Wiley-VCH Verlag GmbH, Weinheim, Germany, 2018.
18. Z. Jin, X. Du, Y. Xu, Y. Deng, M. Liu, Y. Zhao, B. Zhang, X. Li, L. Zhang, C. Peng, Y. Duan, J. Yu, L. Wang, K. Yang, F. Liu, R. Jiang, X. Yang, T. You, X. Liu, X. Yang, F. Bai, H. Liu, X. Liu, L. W. Guddat, W. Xu, G. Xiao, C. Qin, Z. Shi, H. Jiang, Z. Rao, H. Yang, Nature 582 (2020) 289–293. https://doi.org/10.1038/s41586-020-2223-y
19. X. Meng, X. Wang, Y. Ma, Y. Wang, Journal of Hazardous Materials 373 (2019) 620–629. https://doi.org/10.1016/j.jhazmat.2019.03.094
20. M. Petukh, E. Alexov, Asian J. Phys. 23(5) (2014) 735–744.
21. J. B. Foresman and Æ Frisch, Gaussian, Inc.: Wallingford, CT, 2015.
22. K. P. Singh, S. Gupta, RSC Advances 4 (2014) 13215. https://doi.org/10.1039/c4ra01274g
23. QSARIS Reference Guide: Statistical Analysis and Molecular Descriptors, Academic Press, San Diego, USA, 2000.
24. F. Buontempo, Genetic Algorithms and Machine Learning for Programmers, Andy Hunt, Raleigh, North Carolina, 2019.
25. D. C. Montgomery, E. A. Peck, and C. G. Vining, Introduction to Linear Regression Analysis Third Edition, Wiley-Interscience, New York, 2001.
26. M. Dehmer, K. Varmuza, D. Bonchev., Statistical Modelling of Molecular Descriptors in QSAR/QSPR, Wiley-VCH Verlag & Co. KGaA, Weinheim, Germany, 2012.
27. TIBCO® Data Science – Workbench an academic license for Statistica 13.6.0, 2020.